ISSN : 0974 - 7486 Volume 10 Issue 8

Materials Science

An Indian Journal

Full Paper

MSAIJ, 10(8), 2014 [339-350]

Barrier properties of polylactic acid /layered silicate nanocomposites for food contact applications

Burcu Şengül[1], Nursel Dilsiz[2]*

[1]Packaging Laboratory, Ankara Food Control Laboratory Directorate, The Ministry of Food, Agriculture and Livestock, Yenimahalle 06170 Ankara, (TURKEY)

[2]Department of Chemical Engineering, Faculty of Engineering, Gazi University, Maltepe 06570 Ankara, (TURKEY)

E-mail : ndilsiz@gazi.edu.tr

ABSTRACT

Polylactic acid/layered silicate nanocomposite films, intended to use as food contact material, are prepared by solution casting technique. Four types of organo modified montmorillonite and an unmodified bentonite are used as inorganic filler. The structural characterizations are performed by FTIR/ATR and dispersion of the layered silicates was determined by XRD. Clay layers are found to be dispersed in the matrix polymer, although agglomerated particles are also detected. DSC study showed that a small amount of organo modified clay is enough to serve as a nucleating agent for crystallization. Surface properties are investigated with dynamic contact angle measurements. All of the nanocomposites exhibited improvement of material properties as compared to that of neat PLA. The overall migration tests are studied. PM24 nanocomposite gave the best oxygen barrier property results and migration values due to the compatibility between clay and polymer matrix.

KEYWORDS

Biodegradable;
Clay;
Packaging;
Films;
Biopolymers & renewable polymers.

INTRODUCTION

Huge amounts and different types of plastics, especially polyolefins, polystyrene and poly(vinyl chloride) were produced mainly from fossil fuels, used up and left to the environment, becoming eventually as undegradable wastes[1]. The fact that the nondegradable plastic materials adversly effect the environment with disposable materials. Global concerns are increasing because of the environmantel effect of continuous plastic wastes, but alternative disposal methods are restricted. Plastic waste incineration always produce a big deal of carbon dioxide and sometimes generates toxic gases that causes global warming and global pollution[2]. Furthermore the petroleum resources are not infinite. It is being understood to a greater extent that the use of long-lasting polymers for short-lived applications is not convenient[3]. To avoid the effect of plastic wastes, biodegradation and bio-recycling are attractive solutions[4]. The development of green polymeric materials which don’t involve the use of toxic or noxious component in their production and could degrade in the natural environmental products, is becoming important. Because of these reasons, all around the world today, biodegradable material investigations attract attention and has been a subject of materials scientists and engineers[5].

Polylactides or poly(lactic acid) (PLA) is one of the most promising materials among the renewable source-based biodegradable plastics because it is thermoplastic, biodegradable, biocompatible and has high-strength, high-modulus and good processability. The application of PLA has been broaden to other fields such as packaging, textiles and composite materials[6]. With the help of its biodegradation perform, PLA shows a great benefit that when entered in the natural cycle, it returns to the biomass. However, PLA-based materials shows poor properties which include thermal stability and gas barrier properties are still need to be developed to accomplish necessities for food packaging applications. For several years layered silicates for example montmorillonite or hectorite attract great attention in the field of polymer nanocomposites[7,8]. It is often needed to convert the clay more compatible with the organic polymer matrix in order to attain this nanoscale distribution. The 2:1 layered aluminosilicates like montmorillonite, are widely used for the preparation of such nanocomposites. The hydrophilicity of the natural montmorillonite-Na^+ hinders its delamination with the most common hydrophobic polymer matrices. In order to make montmorillonite compatible with polymers, exchange of the sodium cations by more hydrophobic ions, such as alkylammonium cations for example, can easily be acquired in aqueous suspension. Two extreme structures can be described related with distribution/dispersion of the stacks of aluminosilicate layers can be described: The former is an intercalated structure when a regular stacking of polymer layers occures and the latter is an exfoliated structure if the silicate layers are completely and homogeneously delaminated and dispersed in the polymer matrix[9]. With a high aspect ratio (100–1500) and extremely high surface-to-volume ratio (700– 800 m^2/g), the nanoscale distribution of nanoclays constituted important developments to the polymer matrix regarding mechanical, gas barrier, and optical properties at low filler content (less than 5% by weight)[6,7,10,11].

To supply the best protective properties, the food packaging material has to keep its satisfactory for its expected shelf life[12]. With the usage of the PLA as the polymer matrix, it is aimed to accomplish an environmentally polymer composite that could have material properties appropriate for food packaging end-use. That's why, we attempt in this work to prepare films with PLA and five types of clay by using solution casting technique and to investigate the effect of the type of clay on the properties of the prepared films as a food contact material.

All of the nanocomposites showed an improvement of material properties as compared to that of neat PLA film. XRD results showed that prepared nanocomposites exhibited flocculated, intercalated and exfoliated strucure. The highest cyrstallinity degree was obtained % 28. Overall migration tests were studied with food simulants include distilled water, 3 % acetic acid, 95 % ethanol. The migration values of all the prepared films were below the allowed limit (10 mg/dm^2). The best result in oxygen gas transmission rate and water vapor transmission rate were 233,41 cm^3 mm/m^2 day MPa and 98,30 g/m^2 day, respectively. It is observed that oxygen barrier property increased % 34 and water vapor barrier property increased % 65 when compared to neat PLA film.

EXPERIMENTAL DETAILS

Materials

PLA (Natureplast PLE 005) was supplied by Nature Plast.,France with a density of 1.25 g/cm^3. Three commercial clays were received from Sigma Aldrich. Chloroform ($CHCl_3$) was also obtained from Sigma Aldrich. The surfactants with various molecular structures are summarized in TABLE 1.

TABLE 1 : Surface modifications of organoclays

Clay type	Surface modification agent
B59	None
M24	35-45 wt. % dimethyl dialkyl (C14-C18) amine
M32	0.5-5 wt. % aminopropyl triethoxysilane, 15-35 wt. % octadecylamine
M8	Distearyldimethyl ammonium chloride
M40	25-30 wt.% methyl dihydroxyethyl hydrogenated tallow ammonium

B59 is a hydrophilic bentonite. M32 is modified by a primary amine containing silane with a single tail. Ammonium salts with two alkyl (tallow) tails used as a surfactant for M40 clay. Surfactant of M40 has hydroxyl group attached to either the tallow tail or the ammonium head. The hydroxyl group has significant effect on the properties and structure of the composites. Ternary amine with two alkyl (tallow) tails used as a surfactant in the M24 clay. M8 is modified by ammonium salt with a single alkyl (tallow) tail.

Preperation of nanocomposites

PLA and clays were dried under vacuum at 80 ^{o}C for 3 hours prior to use. PLA and PLA-based nanocomposite films were prepared by using a solvent casting method[13-16]. 0,5 grams of PLA was dissolved in chloroform while mixing vigorously at room temperature to prepare 5% solution. This solution was poured onto a glass petrie dishe and then allowed to dry for about 5 days at room temperature. The resultant film was peeled from the casting surface. For the preparation of PLA nanocomposite films, a predetermined amount of clay was dispersed in the solvent by vigorous stirring for 1 h using a magnetic stirrer, followed by sonication for 2 h at room temperature. The nanoclay solutions were mixed with the previously prepared PLA solution, sonicated for 30 minutes, cast onto the glass petrie. PLA/nanoclay films were prepared with different types of nanoclays (B59, M32 and M40, M8 and M24). In this study clay percentage was kept constant at 3 wt.%. After drying at room temperature for about 5 days, all PLA films were peeled from the casting surface.

Characterization

The chemical composition of the nanocomposite films was determined by a Tensor 27 Bruker Fourier Transform Infrared Spectrometer (ATR-FTIR) instrument with the spectral range of 4000-550 cm^{-1} and resolution of 16 cm^{-1}.

Dispersibility of clays in polymer matrix was investigated by using X-ray diffraction analyses. XRD was performed on samples with a Rigaku Ultima IV X-Ray Difractometer in the range 2θ=0-40 ^{o} at 2^{o}/min scanning rate at room temperature.

Differential scanning calorimeter (DSC) from Setaram, Setsoft 2000 Instruments was used to determine Tg, Tm and enthalpies. The crystallinity of polymers was calculated from the enthalpies. Heating procedure was applied from 25 to 200 ºC at a heating rate of 10ºC/min. The glass transition temperature (T_g), melting temperature (T_m) and melting enthalpy (ΔH_m) were measured at argon atmosphere. The percent of crystallinity, χ_c, can be evaluated as follows:

$$\chi_c = (\Delta H_m / \Delta H^c_m) * 100$$

where Hm is the melting enthalpy H^c_m =93 J/g is the heat of melting of pure crystalline poly(L-lactide)[17-20].

Surface properties of the films were investigated with contact angle measurements. Sessile drop contact angle measurements using Krüss100 DSA were performed dynamically using a motor-driven syringe to pump liquid steadily into the sessile drop from below the surface. Critical values of the advancing and receding contact angles were measured at room temperature. The arithmetic difference relation was used to calculate contact angle hysteresis: $H = \theta a - \theta r$

Oxygen gas transmission rates of PLA and nanocomposites were measured at 23 °C and 0% relative humidity by the ASTM D3985 with Sytech Instruments 8001.

Water vapor permeability of PLA and nanocomposites were carried out at 38^{o}C and %90 relative humidity by the ASTM E96 with Sytech Instruments 7000.

Overall migration tests of films were done according to EN 1186; plastic materials and articles intended to come into contact with foodstuffs[21]. The tests were carried out with three different food simulants (distilled water, 95% ethanol and %3 acetic acid) for 10 day at 40 ^{o}C.

RESULTS AND DISCUSSION

FT-IR/ATR spectra of PLA and composites

The infrared spectrum of neat PLA film was determined by FT-IR/ATR Spectroscopy. FT-IR/ATR spectrum and band assignment for neat PLA film were given in Figure 1 and in TABLE 2, respectively.

The principal PLA absorption bands are summarized in TABLE 2. The strong IR bands at 3000, 2948 and 2877 cm^{-1} are assigned to the CH stretching region, $\nu_{as}(CH_3)$, $\nu_s(CH_3)$ and ν(CH) modes respectively. The C=O stretching region is observed as a strong band at 1747 cm^{-1}. The band at 1456 cm^{-1} is due to CH_3 bending mode. The CH deformation symetric and asymmetric bands appeared at 1382 cm^{-1} and 1360 cm^{-1}, respectively. The bands that appear at 1315 cm^{-}

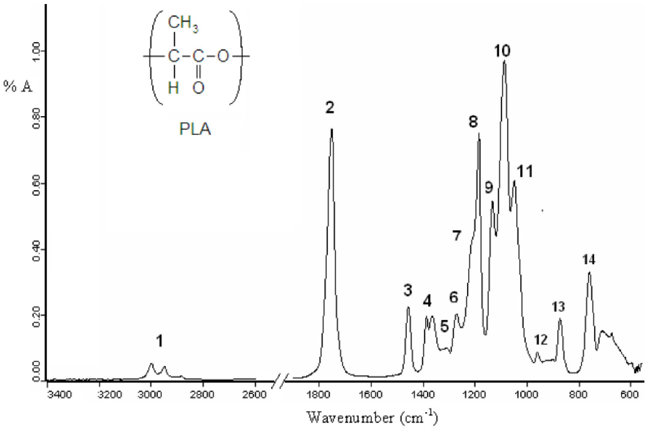

Figure 1 : FT-IR/ATR spectrum of neat PLA film

TABLE 2 : Peak band assignment for neat PLA film

Peak number	Assignment	Wavenumber (cm^{-1})
1	-CH- strech	3000,(asim), 2948 (sim), 2877
2	-C=O carbonyl strech	1747
3	-CH$_3$ bend	1456
4	-CH- asymetric ve smetric deformation bend	1382,1360
5	-CH- bend	1315-1300
6	-C-O- strech	1265
7	-C=O bend	1211
8,9,10	-C-O- strech	1180, 1129, 1083
11	-CO strech	1044
12	-CH$_3$ rocking mode	955, 916
13	-C-C- strech cyrstalline phase	869
14	amporphous phase	755

^{1} and 1300 cm^{-1} are due to the CH bending modes. The C–O stretching modes of the ester groups at 1225 cm^{-1} was observed as a shoulder on the band of 1185 cm^{-1} and about 1211 cm^{-1}. The bands at 1180, 1129 and 1083 cm^{-1} are due to C-O stretching mode. The band at 1044 cm^{-1} is based on CO stretching mode. The peaks appear between 1000 cm^{-1} and 800 cm^{-1}, 955 cm^{-1} and 916 cm^{-1} which can be attributed to the characteristic vibrations of the helical backbone with CH$_3$ rocking modes. The band at 869 cm^{-1} 755 cm^{-1} are related to the crystalline and amorphous phases of PLA, repectively[22-25].

FT-IR/ATR spectra was obtained in the spectral range of 4000-550 cm^{-1}. For neat clays the peak at 3632 cm^{-1} is due to ν(O-H) stretching vibration based on H_2O[26,27]. In the spectra of M32 clay the broad peak near 3250 cm^{-1} reflects the ν(N-H) stretching vibrations and it is an indication that the surfactant in the modified clay has amine groups[28]. So, the peak at 3250 cm^{-1} could be used to distinguish the type of surfactant employed. It is noted that all modified clays exhibit peaks at 2925 and 2850 cm^{-1} due to CH$_2$ and CH$_3$ symmetric and asymmetric stretching related to surface modification[26-31]. Due to modifier of M40 clay has two hydroxyl groups, the peak at 1640 cm^{-1} in Figure 2.c is due to δ(H-O-H) stretching vibrations the similiar peak is also seen very slightly in Figure 3.c[28]. The peak at 1609 cm^{-1} and broad peak between 1569-1494 cm^{-1} are due to N-H stretching vibrations which is also assigned to amine groups[28]. in the spectra of M32 clay (Figure 2.b), but these peaks were not detected in M24 and M8 clay because of the weak N-H stretching vibrations of ternary amine and ammonium salt[28]. The peak at 1466 cm^{-1} is due to δ(CH$_2$) bending vibrations[28]. The typical stretching vibrations of bentonite appear at 1107 and 993 cm^{-1}[26,32] and the improvement of the peak at 1037 cm^{-1} is due to this stretching vibration. This peak is overlapped with CO stretching vibration (1044 cm^{-1}) of neat PLA film.

The typical bands for oxydes are assigned to the peaks of Si–O– Si, Si–O–Al and Si–O–Mg stretching around 1050 cm^{-1}[28,32]. These bands can be seen at 1028, 1008 cm^{-1} for M32 clay, at 1115 and 1024 cm^{-1} for M40 and M8 clay, 1115 and 1044 cm^{-1} for M24 clay, respectively. These peaks are overlapped with CO stretching vibration at 1044 cm^{-1} of PLA neat. The Al-Al-OH deformation vibration peaks about at 917 cm^{-1}[27]. which are related to clays is also seen in the IR spectra of nanocomposite films. The peak intensity which is related to cyrstalline phase of PLA is increased in the P-B59-3 and P-M24-3 nanocomposites at %3 clay loading. Both amorphous and crystalline structure of PLA were not affected significantly at 3% clay loading.

Dispersibility of clays in PLA

Hydrophilic clays and hydrophobic polymers are not compatible in their original forms. Surface modification of clay is commonly used to reach a greater compatibility of the clay and polymer, which leads to an increase for the d-spacing between silicate interlayers[28].

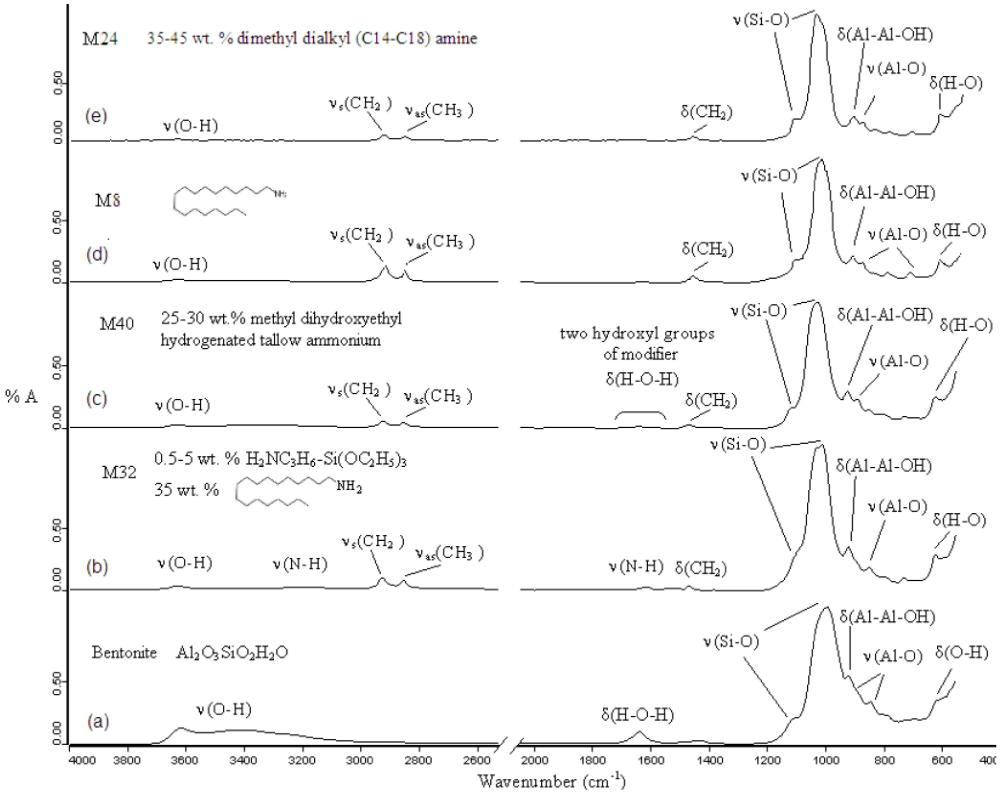

Figure 2 : FT-IR/ATR spectra of (a) B59 clay (b) M32 clay (c) M40 clay (d) M8 clay e) M24 clay

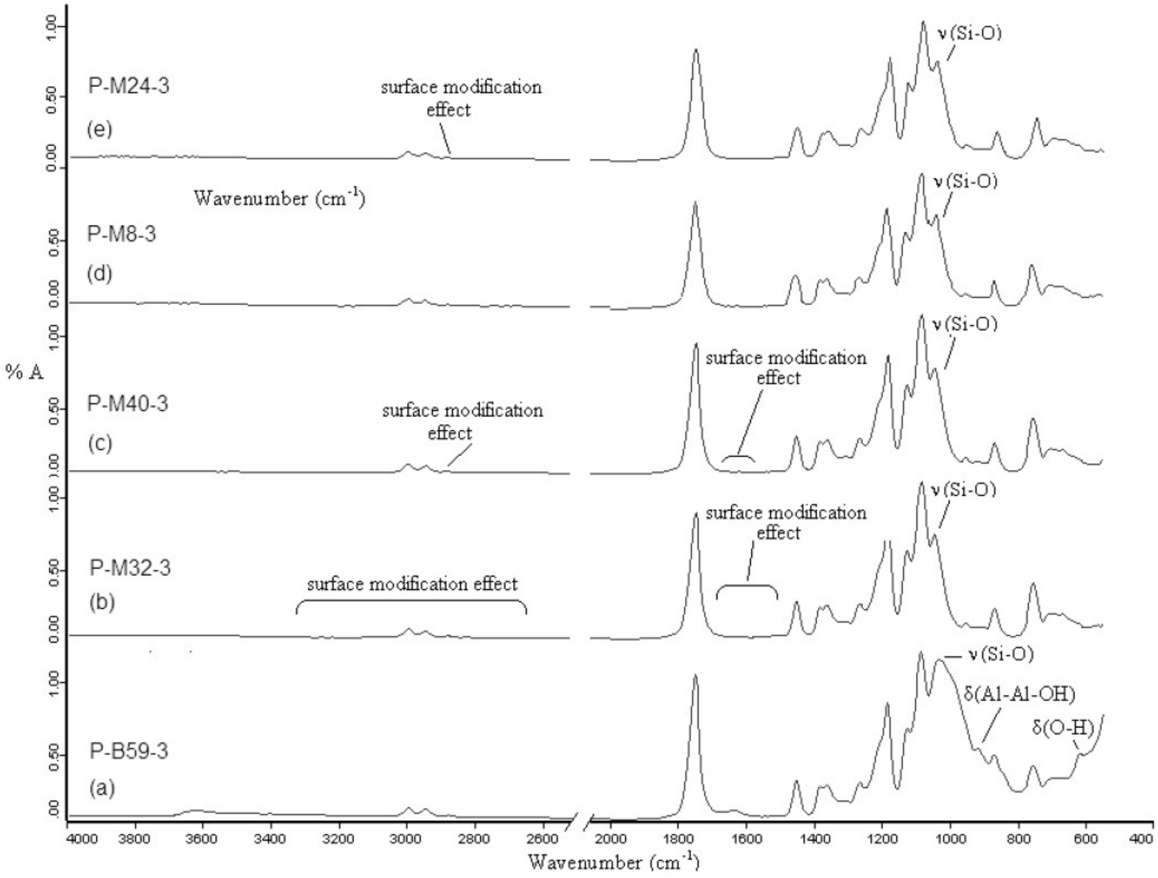

Figure 3 : FT-IR/ATR spectra of (a) P-B59-3 (b) P-M32-3 (c) P-M40-3 (d) P-M8-3 (e) P-M24-3 nanocomposite

If the polymer chains is not intercalated between silicate layers a phase separated composite can be obtained and the poroperties of the prepared composite can not be different from a conventional microcomposites. If the polymer chains are intercalated between the silicate layers, the distance between the well-ordered layers are leading to a shift of the diffraction peak to lower angle values according to Bragg's relation and intercalated structure can be obtained. When the silicate layers are completely dispersed in the polymer matrix, an exfoliated structure can be obtained[33].

Direct evidence of the dispersion of the polymer chains into the silicate layers is provided by the XRD patterns in the range of $2\theta = 1\text{-}40^{\circ}$ as shown in Figure 4.

For pure PLA film the two most intense peaks at $2\theta = 16.62^{\circ}$ and $2\theta = 18.98^{\circ}$, which are ordered α- form and disordered α'-form characteristic peaks of PLA. In addition, for pure PLA films, very small peak at $2\theta = 14.93^{\circ}$ is specific only to α-form of pure PLA. The

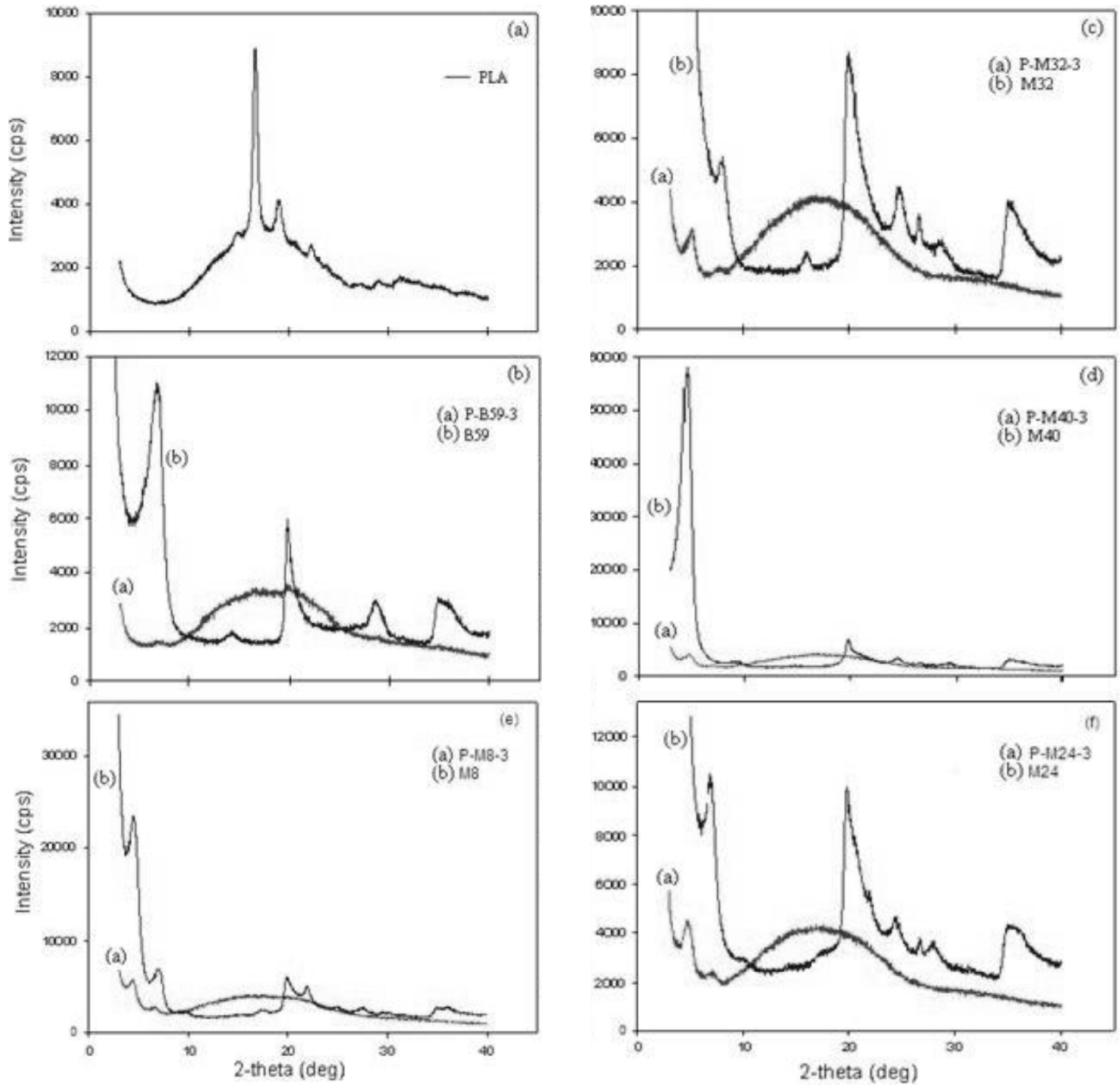

Figure 4 : XRD pattern of (a) pure PLA, (b)B59 and P-B59-3, (c) M32 and P-M32-3, (c) M40 and P-M40-3 (e) M8 and P-M8-3, (f) M24 and P-M24-3

peak at 2θ =21.8° indicating that PLA film contained stereocomplex crystallities[34].

The XRD data (in Figure 4.b) showed that for P-B59-3 nanocomposite the d001 peak 2θ=6.65° of the clay was shifted to higher angle 2θ=6.83° which can be considered as a result of some edge to edge interactions of clay layers. The interlayer distance of this peak decreased from 13.28 to 12.92 °A. Thus, P-B59-3 nanocomposite has a flocculated structure. This is due to the hydroxylated edge–edge interaction of the silicate layers. Owing to the interaction between the clay particles and PLA matrix, the disk– disk interaction also plays an important role in determining the stability of the clay particles.

The XRD data (in Figure 4.c) showed that the d001 peak 2θ=7.93 of the clay was shifted to lower angle 2θ=5.13 for P-M32-3 nanocomposite. The interlayer distance of this peak increased from d= 11.14 A° to d= 17.18 A°. Thus, P-M32-3 nanocomposite showed an evidence of intercalated structure. The XRD pattern of P-M32-3 represents a very sharp peak, indicating the formation of a well-ordered intercalated nanocomposite. The nanocomposite P-M32-3 had no other peak in the diffractogram exhibiting an evidence of exfoliated structures.

The XRD data (in Figure 4.d) showed that the d001 peak 2θ =4.72° of the clay was shifted slightly to higher angle 2θ =4.86° for P-M40-3 nanocomposite. The interlayer distance of this peak decreased from 18.69 A° to 18.15 A° due to flocculated organoclay particles. P-M40-3 nanocomposite had no another peak in the diffractogram giving an evidence of exfoliated structures.

The XRD data (in Figure 4.e) showed that the d001 peak 2θ =4.35° of the clay was shifted slightly to higher angle 2θ =4.86° for P-M8-3 nanocomposite. The interlayer distance of this peak decreased from 20.29 A° to 19.90 A°. It is due to flocculated structure of this clay. However, d002 peak 2θ =7.06° of the clay was shifted to lower angle 2θ =6.6° and the interlayer distance of this peak increased from 12.51 A° to 13.3A° giving an evidence of intercalated structure. Thus, P-M8-3 nanocomposite gave an evidence of intercalated structure. The diffractogram of this nanocomposite has no other peak, giving an evidence of exfoliated structure. This nanocomposite included three kinds of dispersibility.

The XRD data (in Figure 4.f) showed that the d001 peak 2θ =7.05° of the clay was shifted to lower angle 2θ =4.86° for P-M24-3 nanocomposite. The interlayer distance of this peak increased from 12.53 A° to 18.12 A°. Thus, P-M24-3 nanocomposite shows an evidence of intercalated structure. XRD pattern of P-M24-3 indicated the formation of a well-ordered structure. The diffractogram of this nanocomposite has no other peak giving evidence of exfoliated structure.

Among the clays tested, B59 clay exhibited the worst interaction with the hydrophobic PLA polymer matrix as evidenced by XRD patterns.

Thermal properties

The DSC thermograms of blends of PLA with different organic modifiers were listed in TABLE 3.

An endothermic peak for PLA was observed at 49.34 °C in Figure 5. Increase in T_g value was reported for P-B59-3. This behavior has been explained with the nature of tie molecules between crystallites should have played a role, as some increase in T_g value was observed for P-B59-3, in which a phase-separated structure was formed[35]. DSC does not detect any traces of thermal transitions for P-M32-3, P-M24-3 and P-M40-3.

TABLE 3 : DSC termograms of PLA and nanocomposites

	T_g (°C)	T_c (°C)	ΔH_c (J/g)	T_M (°C)	ΔH_m (J/g)	χ_c (%)
PLA film	49,34	91,13	14,79	151,90	22,35	24
P-B59-3	52,02	101,49	20,51	151,12	24,52	26
P-M32-3	-	79,99	7,80	149,97	23,13	25
P-M40-3	-	79,02	7,09	151,10	25,76	28
P-M24-3	-	89,50	16,18	150,06	24,89	27
P-M8-3	47	89,50	16,18	150,06	24,89	27

The DSC study showed that the Tg signal of neat PLA disappeared when organo modified clay added. This behavior suggests that clay layers effect polymer matrix and there is no amount of bulklike PLA present[2,36].

On the other hand, all nanocomposites gave an exothermic peak that can be related with the crystallization of PLA in every sample; the corresponding tempera-

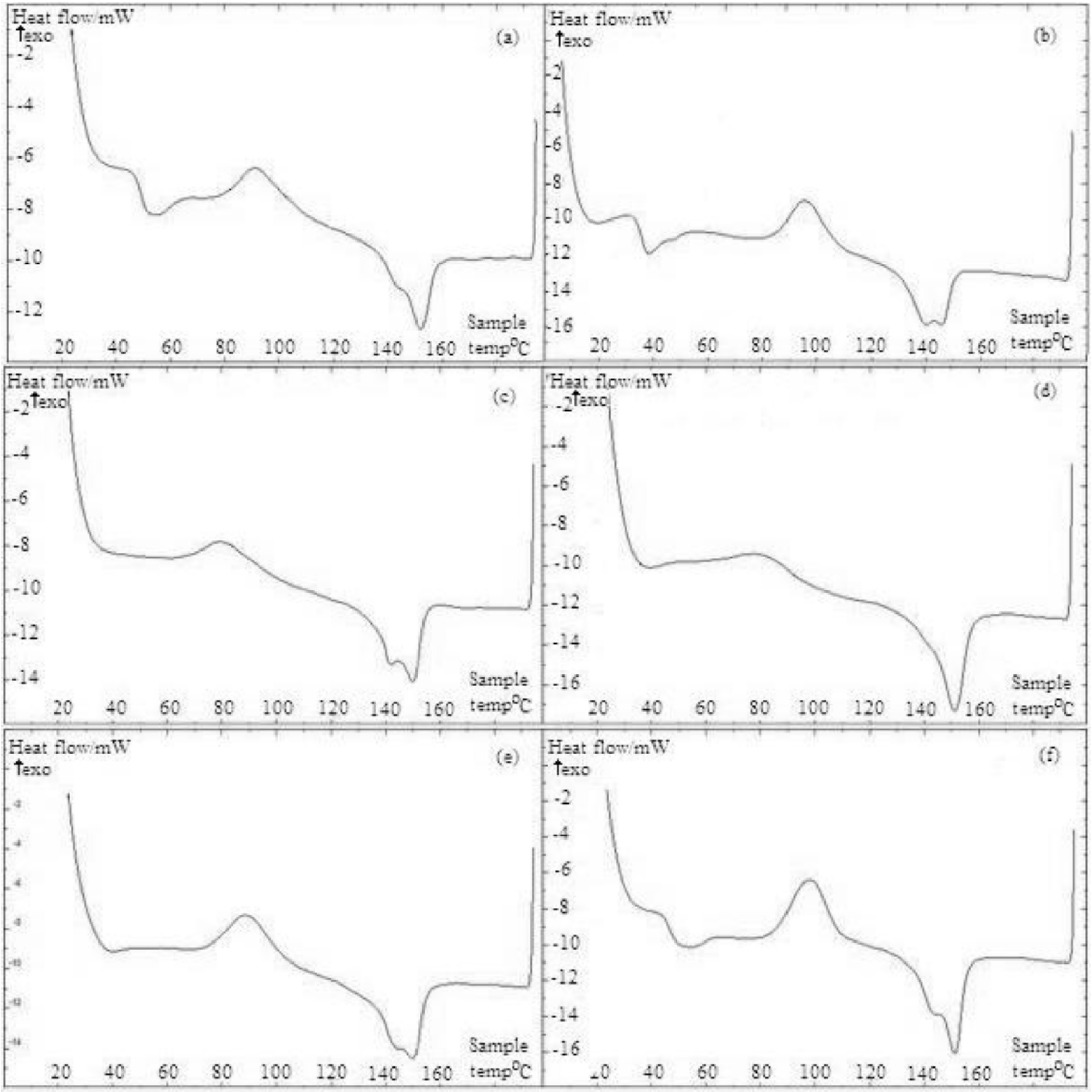

Figure 5 : DSC thermogram of (a) pure PLA, (b) P-B59-3, (c) P-M32-3, (d) P-M40-3 (e) P-M24-3 (f) P-M8-3

ture is known as the crystallization temperature, T_c [2,23,37]. T_c decreased with organo modified clay, indicating pronounced nucleating behavior of modifier. In the case of nanocomposite's this peak appeared at lower temperature than that of neat PLA except P-B59-3. Therefore, the organo modified clay seems to enhance the rate of crystallization of PLA. It is noted that T_c is strongly depend upon the nature of organo modified clay. This behavior suggests that a small amount of organo modified clay is enough to serve as a nucleating agent for crystallization[2,20].

The peak temperature of melting of pure PLA film was shifted very sligthly to low temperatures. The crystalline phase content calculated under the curve that the melting enthalpy of the 100% crystalline PLA is 93 J/g[17,36,38]. The degree of crystallinity increased from 24% (pure PLA) to 26% (P-B59-3), 25% (P-M32-3), 28% (P-M40-3), 27% (P-M24-3), 27% (P-M8-3). It has been reported that the presence of multiple melting peaks in nanocomposites is related to the formation of different crystal structures[4].

Surface properties

The contact angle is an important parameter in surface analysis. It is a common measure of the hydrophobicity of a solid surface. The upper limit of the range is the advancing contact angle, θ_a, which is the contact angle found at the advancing edge of a liquid drop. The lower limit is the receding contact angle, θ_r, which is the contact angle found at the receding edge. The difference between the advancing and receding contact angles is known as the contact angle hysteresis,

$$H = \theta_a - \theta_r$$

The contact angle shows hysteresis due to the roughness and heterogeneity of a solid surface[39,40]. The dynamic contact angle value of nanocomposite films were given in TABLE 4. The hysteresis value of the nanocomposite films was found increased with clay content. The hysteresis of all the nanocomposite films were lower than P-B59-3 nanocomposite film. This is due to weak interaction between B59 clay and polymer matris than organo modified clays.

TABLE 4 : Dynamic contact angle values

	Advancing, θ_a	Receding, θ_r	Hysteresis
PLA	89,5±0,20	77,2±3,43	12,3
P-B59-3	83,5±1,11	57,4±2,12	26,1
P-M32-3	91,4±2,24	70,1±1,31	21,3
P-M40-3	91,0±0,89	65,8±3,43	25,2
P-M8-3	93,9±0,80	69,4±0,86	24,5
P-M24-3	91,2±0,48	69,4±0,86	21,8

Barrier properties

Oxygen gas barrier properties

O_2 gas permeability coefficients of neat PLA and nanocomposites were presented in TABLE 5. As expected, the barrier property of the nanocomposite was higher than that of neat PLA film.

The permeability of nanocomposites significantly depends on dispersed layered silicate particles dimension and dispersion of layered silicate in polymer matrix[20]. All of the composite films improved the oxygen barrier property when compared to neat PLA. P-M24-3 nanocomposite indicated exfoliated-intercalated structure from the XRD patterns, enhanced the oxygen barrier property of neat PLA (34%). PM8 nanocomposite which had exfoliated-intercalated-flocculated structure of the nanocomposite showed 29% increase in oxygen barrier property. It is suggested that the significant increase in oxygen barrier property of P-M40-3 nanocomposite (28%) can be related with the interactions between PLA and M40 nanoclay containing hydroxyl group modifier and the high cyrstallinity degree of P-M40-3 nanocomposite. It was concluded that the surface modifer ternary amine with two alkyl (tallow) tails (M24 clay) was much more effective in reducing O_2 gas permeability.

TABLE 5 : Oxygen gas transmission rates of PLA and nanocomposites

	O_2TR cm^3 mm/m^2 day MPa	% improvement
	23°C , %0 relative humudity	
PLA	355,90	
P-B59-3	310,64	13
P-M32-3	264,00	26
P-M40-3	256,60	28
P-M8-3	251,86	29
P-M24-3	233,41	34

Water vapor barrier properties

The potential for enhanced barrier performance of the nanocomposite films relative to the neat films is a reflection of the large aspect ratio and surface area of the nanoclay. When the silicate layers dispersed succesfully, these layers may form a 'tortuous pathway' that water molecules must follow in the composite film. The degree of tortuosity also indicates geometrical influences such as the shape and state of exfoliation/intercalation of the platelets and their orientation in the polymer matrix[41]. Water vapor permeability (g /m^2 day) for neat PLA and nanocomposite films were presented in TABLE 6.

In all cases, the nanocomposite films showed lower water vapor permeability than the pure PLA films, exhibiting 65% reduction in water vapor permeation rate with M40 clay. The increase in water vapor barrier property of polymer/clay composite films is mainly attributed to the tortuous path for water vapor diffusion due to the impermeable clay layers distributed in the polymer matrix consequently increasing the effective

TABLE 6 : Water vapor permeability of PLA and nanocomposites

	WVTR g/m^2 day	% improvement
	38^{o}C, %90 relative humudity	
PLA	278,00	-
P-B59-3	138,00	50
P-M32-3	143,00	49
P-M40-3	98,30	65
P-M8-3	107,00	62
P-M24-3	109,00	61

diffusion path length. In this study, the WVP of nanocomposite films changed significantly depending on the type of nanoclays used. M40 clay was more effective in reducing WVTR than others. This result also indicates that M40 has favorable interactions with PLA polymer matrix.

Migration

Lactic acid, lactoyllactic acid, other small oligomers of polylactide and lactide may be included in migrants from PLA. In this study, total migration tests were carried out according to EN 1186; plastic materials and articles intended to come into contact with foodstuffs. PLA was stored for 10 day at 40 °C with three different food simulants, 95% ethanol, 3% acetic acid and distilled water.

The total amount of migrants that migrates from the film is given in TABLE 7. It is expected that lactic acid and its derivates migrates from PLA to the food simulants. Lactic acid is the most interesting and significant substance because all the other species are finally hydrolized to lactic acid. According to the overall migration results, the migration values were below the allowed limit (10 mg/dm^2) and lower than lactic acid intakes values reported by the Food and Drug Administration. Due to the interactions between M24 clay and PLA matrix, PM24 nanocomposite showed best migration result with all of the used simulants.

Nanotechnology for foods and food contact materials has been aroused an interest because engineered nanomaterials have potential hazard[42]. It is still an unknown question whether consumption of foods, which contain transferred particulate nanomaterials, causes an important health risk or not[43,44]. On the other hand, a report showed a positive effect on the migration, in this reprt presence of nanoparticles was found to slow down the rate of migration up to six times[44] . In order to understand about the safety of food contact materias made by nanotechnology, more studies should be done because the relevant data are limited and migration behavior of nanomaterials can be different from the non-nanoforms[42].

TABLE 7 : Migration study results of PLA and nanocomposites

	DS (mg/dm^2)	AA (mg/dm^2)	EA (mg/dm^2)
P	1,14	1,84	2,39
P-B59-3	2,78	2,65	3,11
P-M32-3	2,16	2,50	2,79
P-M40-3	1,94	2,19	2,33
P-M8-3	2,07	2,37	2,40
P-M24-3	1,44	1,98	2,54

CONCLUSIONS

Nanocomposites based on PLA polymer and five different commercial clays were successfully synthesized via solution casting technique. The chemical composition of the nanocomposite films was determined by FT-IR/ATR technique. The evidence of the dispersion of the polymer chains into the silicate layers is provided by the XRD patterns and the results showed that P-B59-3, P-M32-3, P-M40-3, P-M8-3, P-M24-3 nanocomposites exhibited flocculated, intercalated/exfoliated, flocculated/exfoliated, flocculated/intercalated/exfoliated intercalated/exfoliated strucure, respectively. All of the nanocomposites showed an improvement of material properties as compared to that of neat PLA film. The DSC study showed that the T_g signal of neat PLA disappeared when organo modified clay added. This behavior suggests that clay layers effect polymer matrix. T_c decreased with organo modified clay, indicating pronounced nucleating behavior of modifier. The highest cyrstallinity degree was obtained for P-M40-3 nanocomposite. Contact angle measurement shows hysteresis due to the roughness and heterogeneity of a solid surface. The hysteresis value of the nanocomposite films was found increased with clay content. The permeability of nanocomposites significantly depends on dispersed layered silicate particles dimension and dispersion of layered silicate in polymer matrix. It was concluded that the surface modifer which has ternary amine with two alkyl (tallow) tails) was much more effective in reducing O_2 gas permeability (up to 34%). The nanocomposite films exhibiting 65% reduction in water vapor permeation rate with M40 clay. Water vapor barrier property of nanocomposite films changed significantly depending on the type of nanoclays used. Overall migration tests of neat PLA and the nanocomposites were also studied with food simulants include distilled water, 3 % acetic acid, 95 % ethanol. The migration values of the all films prepared was below the allowed limit (10 mg/dm^2). Due to favorable interaction between M24 clay and PLA matrix, P-M24-3 nanocomposite showed best results in overall migration test and oxygen barrier property.

ACKNOWLEDGEMENTS

This work was supported by Gazi University grants 06/2011-07.

REFERENCES

[1] S.S.Ray, K.Yamada, M.Okamoto, K.Ueda; Polymer, **44**, 857-866 **(2003)**.
[2] S.S.Ray, K.Yamada, M.Okamoto, A.Ogami, K.Ueda; Chem.Mater, **15**, 1456-1465 **(2003)**.
[3] N.S.Oliveira, J.Oliveira, T.Gomes, A.Ferreira, J.Dorgan, I.M.Marrucho; Fluid Phase Equilibria, **222,223**, 317-324 **(2004)**.
[4] K.Fukushima, C.Abbate, D.Tabuani, M.Gennari, G.Camino; Polymer Degradation and Stability, **94**,1646-1655 **(2009)**.
[5] S.S.Ray, M.Bousmina; Progress in Materials Science, **50**, 962-1079 **(2005)**.
[6] J.W.Rhim, S.I.Hong, C.S.Ha; LWT - Food Science and Technology, **42**, 612-617 **(2009)**.
[7] M.A.Paul, M.Alexandre, P.Dege´e, C.Henrist, A.Rulmont, P.Dubois; Polymer, **44**, 443-450 **(2003)**.
[8] A.Sorrentino, G.Gorrasi, V.Vittoria; Trends in Food Science & Technology, **18**, 84-95 **(2007)**.
[9] M.A.Paul, M.Alexandre, P.Dege´e; C.Calberg, R.Je´roˆme, P.Dubois; Macromol.Rapid Commun, **24**, 561-566 **(2003)**.
[10] R.Hiroi, S.S.Ray, M.Okamoto, T.Shiroi; Macromol.Rapid Commun., **25**, 1359-1364 **(2004)**.
[11] J.H.Chang, Y.An, G.S.Sur; Journal of Polymer Science: Part B: Polymer Physics, 41, 94-103 **(2003)**.
[12] I.S.J.M.S.Arvanitoyannis; Rev.Macromol. Chem.Phys., **C39(2)**, 205-271 **(1999)**.
[13] H.C.Koh, J.S.Park, M.A.Jeong, H.Y.Hwang, Y.T.Hong, S.Y.Ha, S.Y.Nam; Desalination, **233**, 201-209 **(2008)**.
[14] A.R.McLauchlin, N.L.Thomas; Polymer Degradation and Stability, **94**, 868-872 **(2009)**.
[15] P.C.Srinivasa, M.N.Ramesh, R.N.Tharanathan; Food Hydrocolloids, **21**, 1113-1122 **(2007)**.
[16] A.Giannakas, C.G.Spanos, N.Kourkoumelis, T.Vaimakis, A.Ladavos; European Polymer Journal, **44(12)**, 3915-3921 **(2008)**.
[17] R.A.Auras, B.Harte, S.Selke, R.Hernandez; Journal of Plastic Film & Sheeting, **19(2)**, 123-35 **(2003)**.
[18] E.Nieddu, L.Mazzucco, P.Gentile, T.Benko, V.Balbo, R.Mandrile, G.Ciardelli; Reactive & Functional Polymers, **69**, 371-379 **(2009)**.
[19] R.A.Auras, B.Harte, S.Selke; Journal of Applied Polymer Science, **92**, 1790-1803 **(2004)**.
[20] S.S.Ray, M.Okamoto;, Macromol Rapid Commun., **24**, 815-840 **(2003)**.
[21] BS EN 1186-3: Materials and articles in contact with foodstuffs.Plastics.Test methods for overall migration into aqueous food simulants by total immersion, **(2002)**.
[22] F.Carrasco, P.Pagès, J.Gámez-Pérez, O.O.Santana, M.L.Maspoch; Applied Surface Science, **255**, 6795-6801 **(2009)**.
[23] R.A.Auras, B.Harte, S.Selke;, Macromol Biosci., **4**, 835-864 **(2004)**.
[24] Y.B.Luo, X.L.Wang, D.Y.Xu, Y.Z.Wang; Applied Surface Science, **255**, 6795-6801 **(2009)**.
[25] T.Furukawa, H.Sato, R.Murakami, J.Zhang, I.Noda, S.Ochiai, Y.Ozaki; Polymer, **47**, 3132-3140 **(2006)**.
[26] M.Majdan, O.Maryuk, A.G³adysz-P³aska, S.Pikus, R.Kwiatkowski; Journal of Molecular Structure, **874**, 101–107 **(2008)**.
[27] M.R.Guilherme, L.H.C.Mattoso, N.Gontard, S.Guilbert, E.Gastaldi; Composites: Part A, 41,375–382 **(2010)**.
[28] R.Gu, B.V.Kokta, D.Michalkova, B.Dimzoski, I.Fortelny, M.Slouf, Z.Krulis; Journal of Reinforced Plastics and Composites, **29(24)**, 3566-3586 **(2010)**.
[29] E.Gunister, D.Pestreli, C.H.Unlu, O.Atýcý, N.Gungor; Carbohydrate Polymers, **67**, 358-365 **(2007)**.
[30] M.Majdan; O.Maryuk, A.G³adysz-P³aska, S.Pikus, R.Kwiatkowski; Journal of Molecular Structure, **874**, 101-107 **(2008)**.
[31] Q.Liu; D.A.Spears; Q.Liu; Applied Clay Science,

19,89-94 **(2001)**.

[32] C.Paluszkiewicz, M.Holtzer, A.Bobrowski, **880**,109-114 **(2008)**.

[33] M.Alexandre, P.Dubois, Materials Science and Engineering, **28**,1-63 **(2000)**.

[34] H.Tsuji; T.Tsuruno; Water Vapor Permeability of Poly(L-lactide)/Poly(D-lactide) Stereocomplexes.Macromol Mater Eng., **295**,709–715 **(2010)**.

[35] M.Pluta, A.Galaski, M.Alexandrea, M.A.Paul, P.Dubois; Journal of Applied Polymer Science, **86**:,1497-1506 **(2002)**.

[36] S.S.Ray, K.Yamada, M.Okamoto, K.Ueda; Nanosci Nanotech, **3(6)**,503-510 **(2003)**.

[37] P.Maiti, K.Yamada, M.Okamoto, K.Ueda, K.Okamoto; Chem.Mater., **14**,4654-4661 **(2002)**.

[38] M.Zenkiewicz, J.Richert, P.Rytlewski, K.Moraczewski, M.Stepczyn´ska, T.Karasiewicz; Polymer Testing, **28**,12-418 **(2009)**.

[39] K.Rogers, E.Takacs, M.R.Thompson; Polymer Testing, **24**,423-427 **(2005)**.

[40] C.N.C.Lam, R.Wu, D.Li, M.L.Hair, A.W.Neumann;, Advances in Colloid and Interface Science, **96**:,169-191 **(2002)**.

[41] C.Thellen, C.Orroth, D.Froio, D.Ziegler, J.Lucciarini, R.Farrell, N.A.D’Souza, J.A.Ratto; Polymer, **46**:,11716–11727 **(2005)**.

[42] K.T.Lee;, Meat Science, **86**:,138–150 **(2010)**.

[43] M.Cushen, J.Kerry, M.Morris, M.Cruz-Romero, E.Cummins; Trends in Food Science & Technology, **24(1)**,30-46 **(2012)**.

[44] J.W.Rhim, H.M.Park, C.S.Ha; Progress in Polymer Science, Accepted Manuscript, **(2013)**.